Modification of semifluorinated alkanethiolate monolayers by low energy electron irradiation

S. Frey, K. Heister, M. Zharnikov, M. Grunze,
R. Colorado, Jr., M. Graupe, O.E. Shmakova, T.R. Lee

Angewandte Physikalische Chemie, Universität Heidelberg, Im Neuenheimer Feld 253, 69120 Heidelberg, Germany. E-mail: Michael.Zharnikov@urz.uni-heidelberg.de; Fax: 06221-54 6199; Tel: 06221-54 4921

The low energy electron induced damage in self-assembled monolayers (SAM) formed from semifluorinated alkanethiolates (SFAT) of $CF_3(CF_2)_9(CH_2)_nSH$ (F10HnSH) with different hydrocarbon chain length ($n = 2, 11$ and 17) on polycrystalline gold has been monitored *in-situ* by X-ray photoelectron spectroscopy and angle resolved near edge X-ray absorption fine structure spectroscopy. All investigated SFAT SAMs exhibit qualitatively similar behavior with respect to low energy electron irradiation. Both the fluorocarbon and hydrocarbon parts and the S/Au interface are affected simultaneously. Progressive disordering of initially well-ordered, densely packed SAMs, desorption of film constituents, and chemical changes within the residual film are observed. Desorption of sulfur-containing fragments, which probably include the complete SFAT chains, was only found for F10H2S/Au. The desorbed carbon-containing fragments originate almost exclusively from the fluorocarbon part of the SFAT SAMs. Fluorine desorbs not only as a constituent of the carbon-containing fragments, but through irradiation-induced scission of C–F bonds. The accumulated chemical changes within the residual SFAT films include the complete disappearance of CF_3 tail group, partial transformation of CF_2 moieties into CF entities, appearance of C=C double bonds in the fluorocarbon and hydrocarbon (predominantly) parts, and transformation of the thiolate head groups into new irradiation-induced sulfur species. Some general tendencies in the reaction of SAMs toward electron-irradiation are noticed in full agreement with previous findings for conventional AT SAMs.

1. Introduction

An important issue in the field of self-assembled monolayers (SAMs) is their modification by light, X-ray and electron irradiation. Such a modification, which can also happen unintentionally during the characterization of these systems by conventional spectroscopic techniques, should always be considered.[1-3] For an estimation of the possible beam damage a detailed knowledge of the character and extent of irradiation-induced processes is necessary. Alternatively, a purposeful and intentional modification of SAMs can be performed, which offers a possibility to use SAMs as a resist or chemical template in lithography applications.[4-13]

At present such an understanding has only been achieved for the SAMs of alkanethiolates (AT).[1,2,14-19] These SAMs are comprised of chain-like AT moieties anchoring to the suitable substrate through the thiolate head group.[20-22] On Au(111) the alkyl chains form a $c(4 \times 2)$ modulated ($\sqrt{3} \times \sqrt{3}$) R30° overlayer lattice with a next neighbor separation of ≈ 4.97 Å and a lateral density of 4.65×10^{14} molecules cm^{-2}.[23-27] It has been shown that X-ray[1,2,14] and electron[3,15-19] irradiation of AT SAMs results in a loss of orientational and conformational order, partial dehydrogenation leading to C=C double bond formation, desorption of the film fragments, reduction of the thiolate moieties, and the appearance of a new sulfur species. The issue of electron irradiation was shown to be of major importance because not the primary X-rays but photo- and secondary electrons were found to be largely responsible for the damage to the organic monolayer at X-ray irradiation.[1,3,14] In this context the

electrons of low kinetic energies (up to several tens of eV) are especially interesting because they prevail in an X-ray photoemission spectrum.

The physical and chemical properties of the AT SAMs can be noticeably affected by partial fluorination of the hydrocarbon chain,[28-33] which is mainly related to the larger molecular volume of the fluorocarbon chain. The next neighbor separation in partially fluorinated alkanethiol (SFAT) SAMs on Au(111) was found to be ≈ 5.8 Å which noticeably exceeds this value for conventional AT SAMs.[28,31,34,35]

The modification of SFAT SAMs by electrons is of interest for many reasons. First, the concentration of fluorine is easy to monitor by X-ray photoelectron spectroscopy which became a standard technique to control the electron-induced damage in ultrathin organic layers.[3,18,19] Although the dehydrogenation process can be followed by infrared spectroscopy[16,17] the quantitative interpretation of the experimental data is not so straightforward as compared to XPS. Second, the combination of the high electron affinity of fluorine and the strong hydrophobic character of the fluorocarbon chains make SFAT SAMs a prospective resist for lithographic applications since the wetting properties of these films may be easy tailored by controlled electron irradiation. An additional relevant issue is the electron-induced deterioration of widely used, fluorocarbon-based organic lubricants due to the low-energy electrons evolving at the interface of the rubbing surfaces.

In the present study, we investigated the low-energy electron induced modification of SAMs formed from SFATs $CF_3(CF_2)_9(CH_2)_nSH$ with different hydrocarbon chain lengths
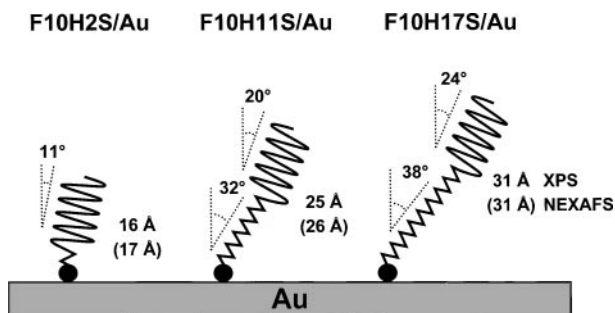
Fig. 1 A schematic drawing of F10H2S/Au, F10H11S/Au and F10H17S/Au. The average tilt angles of the fluorocarbon and hydrocarbon parts and the entire film thickness derived from the XPS and NEXAFS (in brackets) data are marked (see ref. 36 for details).

($n = 2$, 11 and 17: F10H2SH, F10H11SH and F10H17SH, respectively) on polycrystalline gold. This allows a direct comparison of the electron-induced damage in the hydrocarbon and fluorocarbon parts. The structure and chemical composition of these SAMs have been studied by us recently[36] which forms the basis for the current investigation. The results of this recent investigation are summarized in the schematic drawings of F10H2S/Au, F10H11S/Au and F10H17S/Au in Fig. 1. The hydrocarbon and fluorocarbon chains of the adsorbed SFATs retain the expected planar zigzag and helical conformation of the respective bulk materials. The fluorocarbon chains, which are oriented almost perpendicular to the substrate for F10H2S/Au, assume a slightly more tilted orientation in SFAT SAMs with the longer hydrocarbon moieties. These moieties exhibit similar tilt and twist angles to AT chains in conventional AT SAMs. In agreement with the large molecular volume of the helical fluorocarbon chains, a hexagonal arrangement of the SFAT molecules with an intermolecular spacing of 5.8–5.9 Å was found for F10H2S/Au, F10H11S/Au and F10H17S/Au.[34,35] The latter two films are slightly more disordered as compared to F10H2S/Au.[35]

In the following section the experimental procedure and techniques are briefly described. Thereafter, the results are presented and briefly discussed in section 3. A detailed analysis of the data is given in section 4 followed by a summary in section 5.

2. Experimental

The synthesis of F10H2SH, F10H11SH and F10H17SH is described elsewhere.[37] SFAT monolayers were prepared by immersion of polycrystalline gold films (200 nm thickness) evaporated on titanium-primed (20 nm) polished single-crystal silicon (100) wafers (Silicon Sense) in 1 mM thiol solutions in analytical grade dichloromethane.[38] After immersion for 24 h, the samples were carefully rinsed with dichloromethane and blown dry with pure nitrogen.

The SFAT films were irradiated with electrons of kinetic energy of 10 eV. The exposure was varied between 300 and 8000 μC cm^{-2}, the doses were estimated by the multiplication of the exposure time by the delivered current density (about 2.5 μA cm^{-2}). The used flood gun provided a static electron beam. The gun was mounted in a distance of about 15 cm from the sample to assure its uniform illumination. The current density and the homogeneity of electron beam were measured and controlled by a Faraday cup.

Electron induced damage was monitored by angle resolved near edge X-ray absorption fine structure (NEXAFS) spectroscopy and X-ray photoelectron spectroscopy (XPS) in the same UHV chamber where electron irradiation occurred. The combination of these techniques enables one to probe both the occupied and unoccupied states of an organic layer and to monitor its composition, spatial structure and chemical identity. The time for an individual NEXAFS/XPS measurement was selected as a compromise between the signal-to-noise ratio in the spectra and the damage induced by X-rays during spectra acquisition. Control measurements show that the X-ray damage was noticeably smaller than the effect induced by electrons. Only a selected number of exposures, namely 300, 1000, 3000 and 8000 μC cm^{-2} were applied to minimize the entire time of the spectroscopic characterization.

Both the irradiation and characterization were performed at room temperature and at a base pressure better than 2×10^{-9} mbar. The experimental vacuum chamber was attached to the HE-TGM 2 beamline[39] at the synchrotron radiation facility BESSY-1 in Berlin. The NEXAFS spectra were acquired at the C 1s absorption edge with an energy resolution of about 0.65 eV. The measurements were performed in the partial-yield mode with a retarding voltage of -150 V. The angle of light incidence was varied from 90° (the E-vector in the surface plane: normal incidence) to 20° (the E-vector near the surface normal: grazing incidence) to monitor the orientational order within the SFAT films. The corresponding approach is based on linear dichroism in X-ray absorption, *i.e.* the strong dependence of the resonant photoexcitation process on the relative orientation of the light polarization with respect to a molecular orbital of interest.[40]

The raw NEXAFS spectra were normalized to the incident photon flux by division through a spectrum of a clean, freshly sputtered gold sample. For absolute energy calibration the simultaneously measured photoabsorption signal of a carbon covered gold grid with a characteristic resonance at ≈ 285 eV was used. This resonance was separately calibrated by using the NEXAFS spectra of a graphite sample (HOPG), the significant π*-resonance of HOPG being set to 285.38 eV.[41]

The XPS measurements were performed in normal emission geometry. A VG CLAM 2 spectrometer and a Mg-Kα X-ray source, operated at a power of about 260 W and placed at a distance of several centimeters from the samples, were used. The energy scale was referenced to the Au 4f$_{7/2}$ peak at 84.0 eV.[42] For both the pristine and irradiated samples a wide scan spectrum and the F 1s, O 1s, C 1s, S 2p and Au 4f narrow scan spectra were measured. The energy resolution for the C 1s, S 2p and Au 4f regions was about 0.9 eV. The spectra were normalized to the total electron yield to correct for small differences in sample positions and X-ray source intensities. In our experience this procedure works rather well in the case of AT-like SAMs,[18,36] which is explained by the much higher value of the absorption cross section of gold as compared to the corresponding value in alkanethiols.[40] The resulting spectra were fitted by using a Shirley type background[43] and symmetric Voigt functions[44] with variable Gauss and Lorentz contributions. To fit the S 2p$_{3/2, 1/2}$ doublet related to a definite sulfur species we used a pair of Voigt peaks with the same FWHM and Gauss/Lorentz proportion, the standard[42] spin–orbit splitting of 1.2 eV and the intensity ratio of 2 (S 2p$_{3/2}$/S 2p$_{1/2}$).

From the XPS data the effective thickness of the SFAT films was estimated using the intensity ratios of the Au 4f emission for the SFAT-covered and clean gold substrates.[45] An exponential attenuation of the Au 4f signals by the SFAT films was assumed. Because the attenuation length for fluorinated AT SAMs is not known we use the respective value for AT SAMs for the entire SFAT layer: λ(Au 4f$_{7/2}$) = 31 Å.[46,47] At least for the pristine SFAT films this approximation results in the effective thicknesses which are very close to those derived from the orientational information obtained by NEXAFS spectroscopy (see Fig. 1).[36]

No contaminations were observed in the SFAT films. In addition to the XPS and NEXAFS characterization the quality of the pristine SFAT films was checked by infrared reflection absorption spectroscopy.[36]

3. Results

3.1. NEXAFS measurements

NEXAFS experiments provide information about the occurrence and average orientation of the unoccupied molecular orbitals within the organic film of interest.[40] In Figs. 2 and 3 the C 1s NEXAFS spectra recorded at an X-ray incident angle of 55° and the differences of the NEXAFS spectra acquired at X-ray incident angles of 90° and 20° for both the pristine (bottom curves) and irradiated SFAT films, respectively, are presented. Whereas the difference spectra reflect the dependence of the resonance intensities on the incidence angle of the light, the spectra acquired at the magic X-ray incidence angle of 55° exclusively reflect the electronic structure of the unoccupied molecular orbitals of the investigated films and are not affected by the angular dependence of the adsorption cross-sections.[40]

The C 1s NEXAFS spectra for the pristine SFAT SAMs contain two absorption edges at ≈ 287.7 and ≈ 294.0 eV related to the C 1s → continuum excitations for carbon atoms bonded to hydrogen and fluorine, respectively. The spectra are dominated by the pronounced resonances at ≈ 292.5, ≈ 295.5 and ≈ 299.0 eV related to the transition from C 1s state to the C–F σ*, C–C σ* and C–F σ* orbitals of the fluorocarbon part, respectively.[29,30,48] The corresponding transition dipole moments are believed to be oriented almost perpendicular (C 1s → C–F σ*) and along the chain axis (C 1s → C–C σ*).[29,30,48,49] As to the hydrocarbon part, only a noticeable resonance at ≈ 288.0 eV alternatively assigned to the C 1s
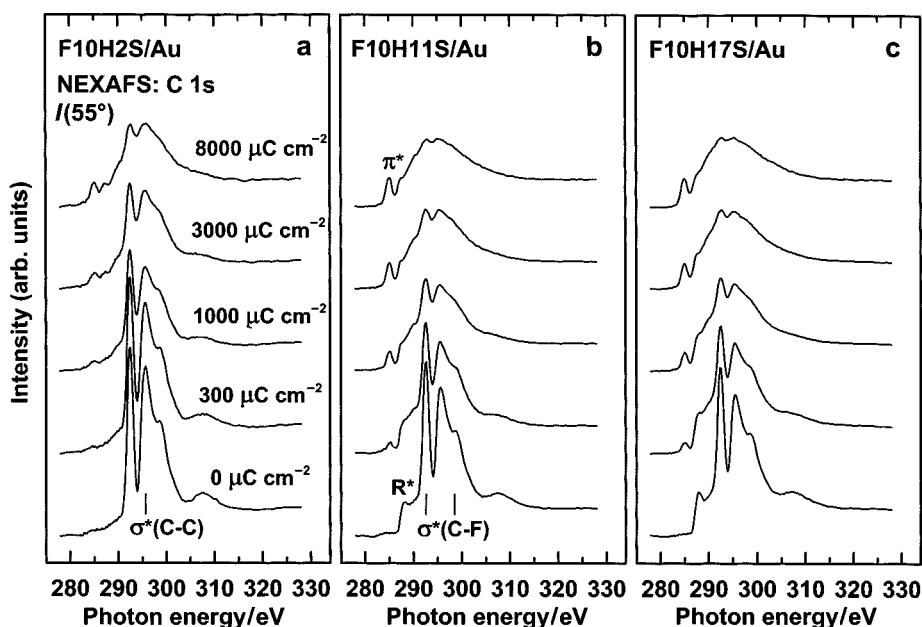

Fig. 2 NEXAFS spectra of the pristine (bottom curves) and irradiated F10H2S/Au (a), F10H11S/Au (b), and F10H17S/Au (c) acquired at an X-ray incident angle of 55°. Characteristic NEXAFS resonances are indicated in (a) and (b).
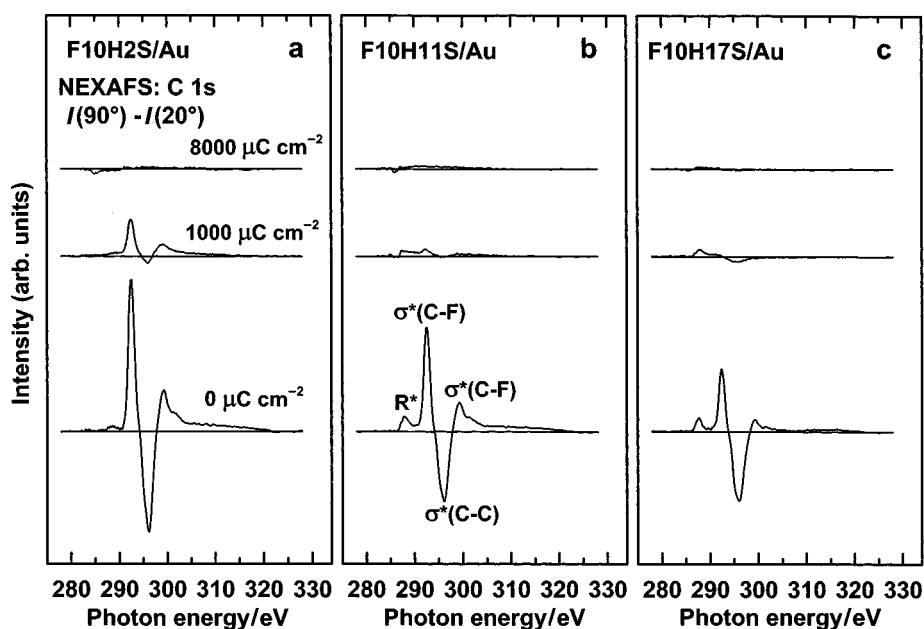

Fig. 3 The differences of the NEXAFS spectra recorded at X-ray incident angles of 90° and 20° for the pristine (bottom curves) and irradiated F10H2S/Au (a), F10H11S/Au (b), and F10H17S/Au (c). The anisotropy maxima related to the characteristic NEXAFS resonances are indicated in (b).
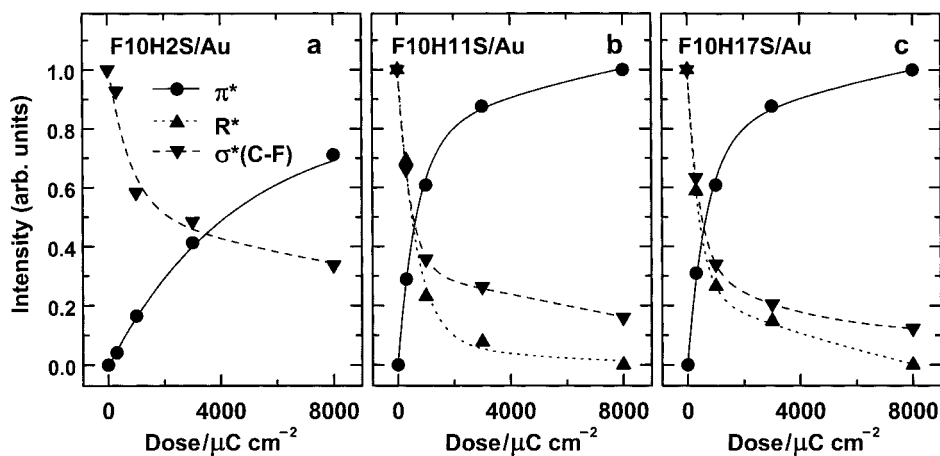
Fig. 4 Intensities of the π* (circles, solid line), R* (up triangles, dotted line), and σ*(C–F) (down triangles, dashed line) resonances extracted from the NEXAFS spectra of F10H2S/Au (a), F10H11S/Au (b), and F10H17S/Au (c) in Fig. 2. The intensities of the R* and σ*(C–F) resonances are normalized to the respective values for the pristine films. The intensities of the π* resonance are normalized to the respective intensity for the strongly (8000 µC cm^{-2}) irradiated F10H17S/Au.

excitations into pure valence C–H orbitals,[40] predominately Rydberg states[50] or mixed valence Rydberg states[51] is observed in the spectra for F10H11S/Au and F10H17S/Au. The characteristic C–C σ* and C–C' σ* resonances of the hydrocarbon part at ≈293 and ≈302 eV, respectively,[49,52,53] overlap with the strong resonances related to the fluorocarbon part and are, therefore, practically non-distinguishable. Consequently, only the resonance at ≈288 eV, which we will denote as an R* resonance (a possible admixture of antibonding C–H σ* orbitals should be, however, taken into account), is representative for the hydrocarbon part of SFAT SAMs. The orbitals related to this resonance are oriented perpendicular to the alkyl chains axis.[49,52,53]

The pronounced linear dichroism of the NEXAFS resonances seen in the difference spectra in Fig. 3 implies well-ordered, densely packed layers. The signs and amplitudes of the anisotropy maxima indicate a predominately perpendicular orientation of both the fluorocarbon and hydrocarbon parts. The tilt of the fluorocarbon segment increases with the length of the hydrocarbon moieties (see ref. 36 for details).

Exposure of SFAT SAMs to 10 eV electrons results in noticeable changes in both the NEXAFS spectra (Fig. 2) and the respective difference curves (Fig. 3). The intensities and angular anisotropy of the NEXAFS resonances decrease with increasing exposure and a new resonance at ≈285.1 eV, which is characteristic for C=C double bonds (π*-resonance) appears (the dose dependences of the π*, R* and C–F σ* resonance intensities are presented in Fig. 4). As in the case for AT SAMs[3,17–19] these changes can be attributed to orientational and conformational disordering, desorption of hydrogen, fluorine, and carbon-containing fragments, and the formation of C=C double bonds in the irradiated films. Strongly irradiated SFAT films are completely disordered (no linear dichroism after irradiation with a dose of 8000 µC cm^{-2}) mixtures of saturated and unsaturated hydrocarbons.

The decrease of the resonances and anisotropy peaks related to the fluorocarbon part is most pronounced, implying that this upper part of the molecule is predominately affected by the electrons. The almost complete disappearance of the corresponding resonances for strongly irradiated SFAT SAMs indicates very extensive desorption of fluorine. Comparison of the spectra in Figs. 2(a), (b) and (c), the difference curves at 1000 µC cm^{-2} in Figs. 3(a), (b) and (c) and the dose dependences of the C–F σ* resonance intensities in Fig. 4 shows,
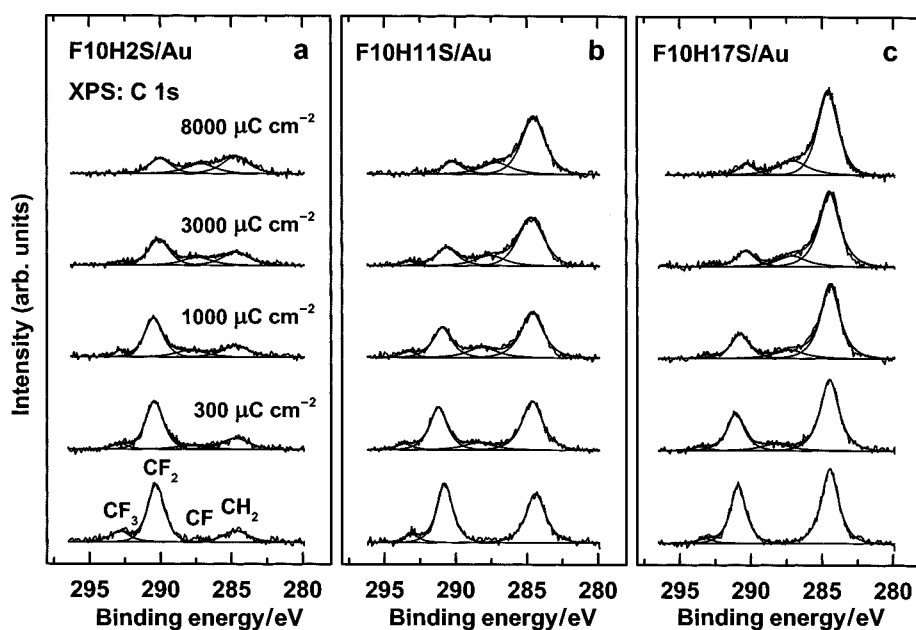

Fig. 5 The C 1s XP spectra of F10H2S/Au (a), F10H11S/Au (b), and F10H17S/Au (c). The bottom curves correspond to the pristine films while the upper spectra are related to the irradiated films. The observed emission peaks are fitted by several Voigt functions.
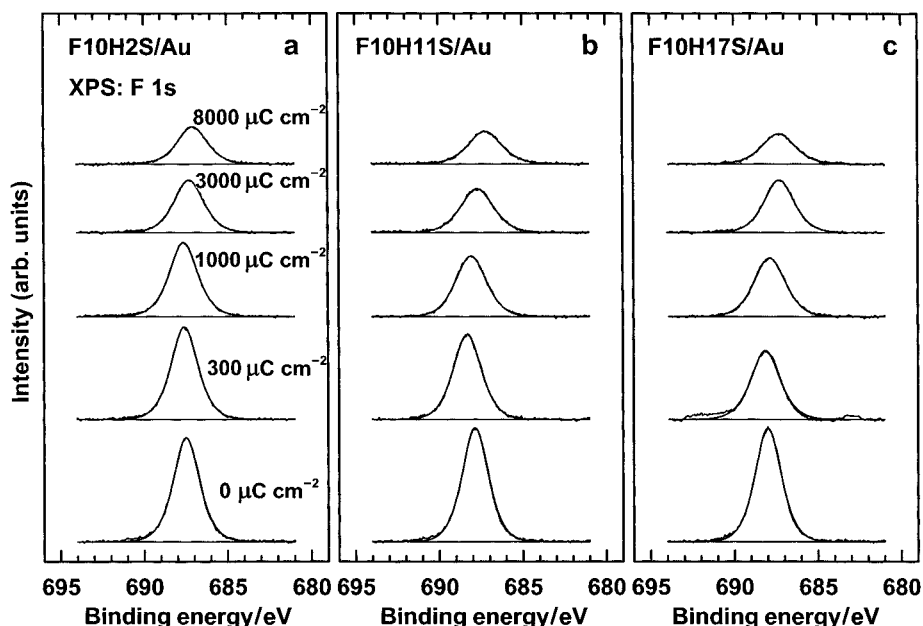
Fig. 6 The F 1s XP spectra of F10H2S/Au (a), F10H11S/Au (b), and F10H17S/Au (c). The bottom curves correspond to the pristine films while the upper spectra are related to the irradiated films. The observed emission peak is fitted by a single Voigt function.

however, that both fluorine desorption and orientational disordering of the fluorocarbon part are less pronounced in F10H2S/Au than in F10H11S/Au and F10H17S/Au. The hydrocarbon parts in the two latter films seem to retain their orientational order longer than the respective fluorocarbon parts. In fact, the relative decrease of the angular anisotropy for the fluorocarbon resonances is stronger than that observed for the hydrocarbon resonances [Fig. 3(b) and (c)]. Interesting is the appearance of the absorption edge related to fluorine-free carbon (≈ 287.7 eV) in strongly irradiated F10H2S/Au (Fig. 2), which reveals extensive desorption of fluorine from the fluorocarbon part. This edge is practically non-distinguishable in pristine F10H2S/Au because of the relatively small portion of hydrogen-bonded carbon.

The formed C=C double bonds have no preferable orientation, which directly follows from the difference curves shown

in Fig. 3. Formation of C=C double bonds occurs noticeably faster in F10H11S/Au and F10H17S/Au as compared to F10H2S/Au, which can be seen in Figs. 2 and 4.

3.2. XPS measurements

Complementary information is provided by the XPS data. The C 1s, F 1s and S 2p XP spectra of F10H2S/Au (a), F10H11S/Au (b) and F10H17S/Au (c) are shown in Figs. 5, 6 and 7, respectively. The intensities of the observed emission peaks are presented in Fig. 8. The thicknesses of the SFAT SAMs derived from the XPS data are depicted in Fig. 9.

In the C 1s XP spectra of the pristine SFAT SAMs in Fig. 5 the emission maxima at binding energies (BE) of 292.7, 290.3 and 284.8 eV related to CF_3, CF_2 and CH_2 entities, respectfully, can be easily distinguished. In agreement with the
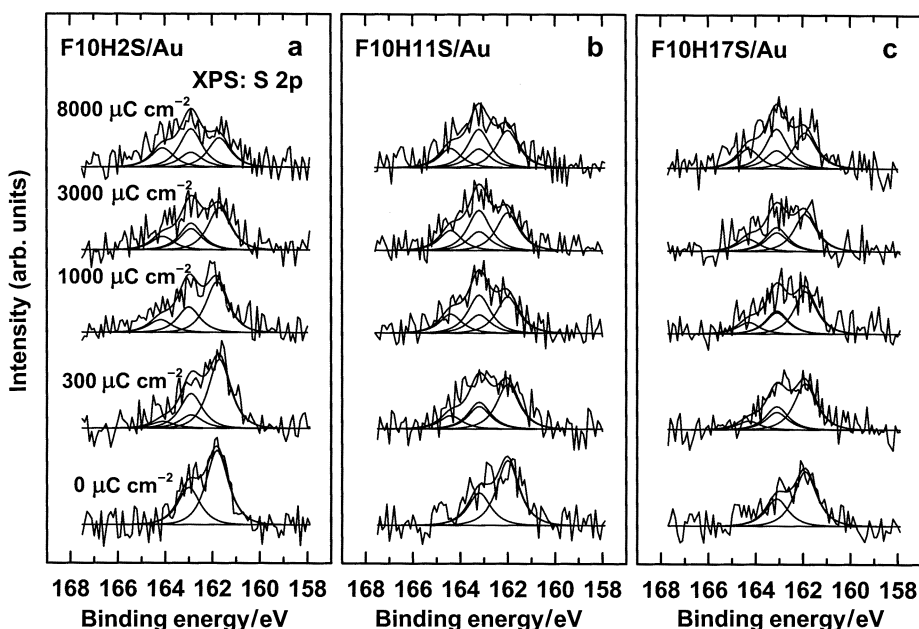

Fig. 7 The S 2p XP spectra of F10H2S/Au (a), F10H11S/Au (b), and F10H17S/Au (c). The bottom curves correspond to the pristine films while the upper spectra are related to the irradiated films. The observed emission structures are fitted by one (for pristine films) or two doublets of Voigt functions (with fixed intensity ratio of $S 2p_{3/2}/S 2p_{1/2} = 2$ and an energy separation of 1.2 eV) related to the pristine thiolate moieties and to a new sulfur species induced by electron irradiation.
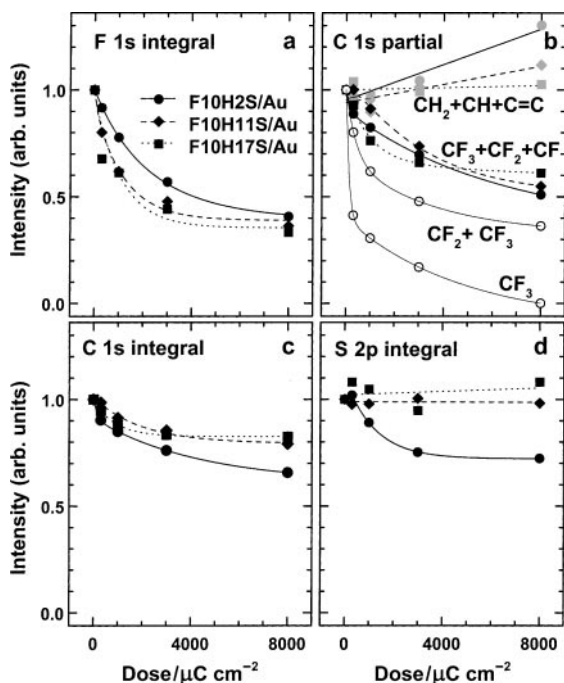
Fig. 8 Intensities of XP peaks for F10H2S/Au (circles, solid line), F10H11S/Au (diamonds, dashed line) and F10H17S/Au (squares, dotted line) derived from the spectra presented in Figs. 5–7. (a) Integral F 1s XP intensity (from Fig. 6); (b) C 1s XP intensity (from Fig. 5) related to the hydrocarbon (grey symbols) and fluorocarbon (black symbols) parts, for F10H2S/Au the contribution exclusively related to CF_2/CF_3 and CF_3 entities are also shown (thin solid line, open circles); (c) integral C 1s XP intensity (from Fig. 5); (d): integral S 2p XP intensity (from Fig. 7). The contributions related to the hydrocarbon parts in (b) and the integral S 2p XP intensity in (d) are corrected for the attenuation by the respective overlayers. All intensities are normalized to the respective values for the pristine SFAT films.

composition of the SFAT SAMs, the intensity of the CH_2-maximum increases with increasing length of the hydrocarbon part, whereas the intensities of the CF_3- and CF_2-maxima remain approximately constant (see ref. 36 for details). In accord with the latter finding similar intensities of the F 1s emission peak are observed for all three pristine SFAT films (Fig. 6). In the S 2p spectra a single S 2p doublet at a BE of
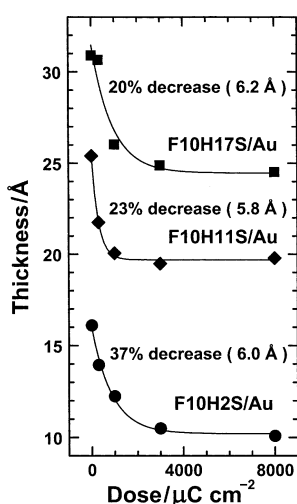

Fig. 9 Dose dependence of the F10H2S/Au, F10H11S/Au and F10H17S/Au film thicknesses. The values were derived from the intensity ratios of the Au 4f emissions for the AT-covered and clean gold substrate. The thickness reductions after irradiation with a dose of 8000 μC cm^{-2} given with respect to the thickness of the pristine films and as absolute values are also presented.

≈ 162.0 eV ($S\,2p_{3/2}$) and ≈ 163.2 eV ($S\,2p_{1/2}$) is observed (≈ 161.8 and ≈ 163.0 eV for F10H2S/Au). This doublet is commonly related to the thiolate species bonded to the gold surface. The positions and FWHM (≈ 1.2 eV) of the $S\,2p_{3/2}$ and $S\,2p_{1/2}$ peaks are essentially the same as for conventional AT SAMs. The low signal-to-noise ratio of the S 2p spectra is related to the attenuation of the corresponding signal by the overlayer and the short acquisition time chosen to minimize X-ray induced damage during the measurement.

The F 1s, C 1s and S 2p XP spectra change with progressive irradiation. The intensities of the F 1s and C $1s_{CF_3/CF_2}$ peaks decrease, this process being less pronounced in F10H2S/Au. These intensities are presented in Figs. 8(a) and (b) (only for F10H2S/Au). A pronounced downward shift of the F 1s and C $1s_{CF_3/CF_2}$ peaks and the appearance of a new C 1s structure at a BE of ≈ 287.5 eV are also observed. This implies irradiation-induced desorption of fluorine leading to a chemical modification of the residual fluorocarbon part of the SFAT SAMs. Considering that a BE of 287.5 eV is very close to the C $1s_{CF}$ BE[29,42,54] the new emission peak in the C 1s spectra can be assigned to CF entities appearing after the loss of one or two fluorine atoms from CF_2 or CF_3 moieties, respectively. Thus, an essential decrease of the fluorine content in the residual fluorocarbon part occurs with respect to the initial composition. Note, that the CF_3 moieties are more strongly affected by electron irradiation than the CF_2 entities. After irradiation with a dose of 8000 μC cm^{-2} almost all CF_3 moieties are destroyed or desorbed, whereas $\approx 35\%$ of CF_2 entities survive [compare the dose dependences of the XP intensities related to $CF_2 + CF_3$ and CF_3 moieties for F10H2S/Au in Fig. 8(b)].

The appearance and increase of the C $1s_{CF}$ peak does not compensate the decrease of the C $1s_{CF_3/CF_2}$ peak. The entire C 1s intensity related to the fluorocarbon part (C $1s_{CF + CF_2 + CF_3}$) decreases with progressive irradiation, which can be clearly seen in Fig. 8(b) where we present the respective dose dependence. Thus, simultaneous to defluorination, desorption of carbon-containing fragments from the fluorocarbon part occurs. The latter process results also in a loss of fluorine through desorption of alkylfluorides. But the entire loss of fluorine prevails over the loss of carbon (with respect to the initial amounts) as mentioned above. This can also be directly seen from the comparison of the dose dependencies of the F 1s and C $1s_{CFx}$ intensities in Figs. 8(a) and (b).

The irradiation-induced carbon desorption from the fluorocarbon part of all three investigated SFAT SAMs is similar. This finding has to be considered together with several other observations such as a similar extent of the thickness reduction in F10H2S/Au, F10H11S/Au, and F10H17S/Au (see Fig. 9) and the almost complete disappearance of CF_3 moieties implying that the part of the SFAT SAMs near the film/vacuum interface is essentially strongly affected by electron-induced processes as compared to the lower part. All these facts suggest that the hydrocarbon part is practically non-affected by the processes leading to the thickness reduction and this reduction is mainly related to the fluorocarbon part. This conclusion agrees also with previous results for conventional AT SAMs[3,17,18] showing that irradiation-induced desorption processes occur predominantly near the film/vacuum interface.

The partial desorption of the fluorocarbon part results in a reduced attenuation of the C $1s_{CH_2}$ XP signal which causes an increase of the respective intensity with progressive irradiation for all three SFAT SAMs (Fig. 5). This effect can be, however, corrected for using the found thickness reduction (Fig. 9) and associating it exclusively with the fluorocarbon part. The corrected C $1s_{CH_2}$ intensities are presented as gray symbols in Fig. 8(b). They remain approximately constant over the applied dosages in agreement with our assumption that the hydrocarbon part is practically non-affected by the processes leading to

the thickness reduction. A small increase of the corrected $C 1s_{CH_2}$ intensities implies that a part of the fluorocarbon chains loses fluorine completely and the resulting "fluorine-free" carbon atoms participate into the $C 1s_{CH_2}$ peak (this process results also in appearance of a low energy absorption edge in the C 1s NEXAFS spectrum for F10H2S/Au as mentioned above). The extent of this process is, however, rather small which follows from only a $\approx 30\%$ increase of $C 1s_{CH_2}$ intensity for F10H2S/Au (with respect to 2 CH_2 entities per chain) and from the lack of the downward energy shift of the $C 1s_{CH_2}$ peak with progressive irradiation.

The total C 1s intensity decreases with progressive irradiation. This decrease is somewhat larger in F10H2S/Au than in F10H11S/Au and F10H17S/Au as seen in Fig. 8(c) where the respective intensities are presented. This can be partly explained by the fact that the loss of carbon almost exclusively occurs at the expense of the fluorocarbon part, which constitutes the major portion of F10H2S/Au. Also the S/Au interface monitored by the S 2p XP spectra (Fig. 7) should be considered in this context. For the irradiated SFAT films the S 2p spectra exhibit the development of a new emission doublet which has been associated with the formation of disulfide species[1-3,18] or/and an incorporation of sulfur into the alkyl matrix through bonding to irradiation-induced carbon radicals in the adjacent aliphatic chains.[3,19] The evolving component was fitted by a standard S 2p doublet (see section 2) with a binding energy of 163.3 eV ($S 2p_{3/2}$) close to that of a disulfide moiety (163.2 eV for $S 2p_{3/2}$)[2] or an alkylsulfide (163.3 eV for $S 2p_{3/2}$).[19,55] The extent of the irradiation-induced sulfur species formation in all three investigated SFAT SAMs is very similar but the dose dependence of the integral S 2p intensity in these systems is noticeably different. In Fig. 8(d) we show the respective intensity changes which have been corrected for the observed thickness reduction. Whereas the S 2p intensities for F10H11S/Au and F10H17S/Au remain approximately constant, the S 2p intensity for F10H2S/Au decreases noticeably. This suggests that the irradiation-induced desorption of sulfur-containing fragments probably including complete SFAT chains does not happen in F10H11S/Au and F10H17S/Au, but does occur in F10H2S/Au.

4. Discussion

The presented NEXAFS and XPS results clearly show the effect of low-energy electron irradiation on SFAT SAMs. As well, the fluorocarbon part, the hydrocarbon part, and the S/Au interface of the initially well-ordered films are damaged.

The strongest changes are observed in the fluorocarbon part of the films. The orientational order in the strongly irradiated SFAT SAMs is completely lost and about 60–65% of the fluorine atoms and ≈ 35–40% of the carbon atoms are desorbed. The desorption of fluorine occurs both directly through C–F bond cleavage and as a constituent of severed alkylfluorides (C–C bond cleavage). The residual portion of the fluorocarbon part becomes depleted of fluorine: the signature of the CF_3 tail groups disappears completely, partial transformation of CF_3 and CF_2 entities into C–F moieties occurs, a small portion of fluorocarbon part (about 5–10%) loses fluorine entirely leading to C=C double bond formation. The desorption processes related to the fluorocarbon part are mainly responsible for the observed thickness reduction. Note that the thickness derived from XPS data resembles the layer thickness given by the occurrence of a definite amount of substance. A SAM compression related to its disordering does not influence the intensities of XP peaks.[3]

The hydrocarbon part also disorders as a consequence of electron irradiation. Both the orientational and conformational order continuously decrease with progressive irradiation and completely disappear in the strongly irradiated

films. This disordering develops, however, at a slower rate as compared to the respective process in the fluorocarbon part. Also some dehydrogenation with subsequent formation of C=C double bonds occurs. A comparison of the NEXAFS spectra for F10H2S/Au, F10H11S/Au and F10H17S/Au in Fig. 2 indicates that the extent of C=C double bond formation in the hydrocarbon part is larger than that in the fluorocarbon part: The intensities of the π^*-resonance for F10H11S/Au and F10H17S/Au are noticeably larger than that in F10H2S/Au. The desorption of carbon-containing fragments from the hydrocarbon part does not occur except for F10H2S/Au where also sulfur is lost.

The S/Au interface becomes damaged in the same way as this happens in conventional AT SAMs exposed to low energy electrons. About 60% of the pristine thiolate moieties transform into a irradiation-induced sulfur species, which can be alternatively assigned to disulfides or alkylsulfides. A noticeable desorption of sulfur-containing fragments probably including the complete F10H2S chains was observed only for F10H2S/Au. This finding correlates well with the results of our previous study[18] on irradiation-induced damage in AT SAMs with different alkyl chain lengths, where we found that desorption of sulfur-containing fragments is influenced by the thickness of the alkyl matrix, being noticeably smaller in the longer-chain films as compared to their shorter-chain counterparts. The main reasons for this phenomena are believed to be the increasing stability with alkyl chain length in the AT SAMs and the trapping of severed fragments within the alkyl layer by carbon radicals.

There are more similarities between the results of the present study and those of previous publications[16,18] indicating general principles in the mechanism of electron induced damage in SAMs. First, the irradiation-induced bond cleavage events leading to subsequent desorption of the severed fragments are predominately localized near the SAM/vacuum interface. The initial bond scission occurs through electronically excited states, which can be quenched through the dipole–dipole coupling with its image on the metal surface.[16,18] The probability of quenching decreases with increasing distance from the metal surface and is smallest at the vacuum interface. But even if a bond scission occurs, cut off fragments can be trapped within the overlayer. The probability of trapping increases with increasing distance from the film surface and is largest for fragments generated near the S/Au interface. Thus, both quenching of electronically excited states and trapping of the severed fragments are most effective at the SAM/metal interface with the result that desorption is most likely at the SAM/vacuum interface. Considering that the irradiation-induced thickness reduction in SFAT SAMs (5.4–6.5 Å) correlates well with that observed for conventional AT SAMs (5.2–6.5 Å)[18] we can assume that the sensitivity of C–C bonds toward electron irradiation is the major factor determining the extent of thickness reduction. It was recently shown that this parameter can be noticeably affected by the incorporation of molecular entities which provide weaker bonds to the adjacent carbon atoms as compared to C–C bond.[19]

Another similarity between conventional AT SAMs and the SFAT films of this study is a stronger resistance of better ordered layers toward electron irradiation. In the case of AT SAMs, films formed on silver demonstrated a higher stability of orientational and conformational order with respect to electron irradiation as compared to the films on gold.[18] The AT SAMs on Ag are known to differ from those on Au through a higher lateral density and a smaller average tilt angle of the alkane chains.[20] In the present study, orientational disordering of the fluorocarbon part and desorption of fluorine from F10H2S/Au developed slower than in F10H11S/Au and F10H17S/Au. This correlates with a smaller ($\approx 12°$ vs. 20–24°) average tilt angle of the fluorocarbon chain and a

higher orientational order in F10H2S/Au as compared to F10H11S/Au and F10H17S/Au.[35,36]

An interesting phenomenon is the desorption of the entire SFAT or AT molecules. A cleavage of the S–Au bond is a necessary (but not sufficient) prerequisite for this process. The extent of this cleavage (monitored by the loss of thiolate species) for both SFAT and AT SAMs is found to be independent of the alkyl chain length. It can be therefore assumed that the SFAT or AT chains do not react as an entire moiety in the case of electronical excitation of S–Au bond.

To provide a qualitative reference for later investigations we have also determined and presented in Table 1 the cross-sections for the observed irradiation-induced processes in SFAT SAMs. Following the formalism of refs. 16 and 18 these processes were described with a standard saturation function

$$I = I_{sat} + (I_{pris} - I_{sat}) \times \exp(-\sigma Q/eS_{irrad}) \qquad (1)$$

where I is the value of a characteristic film parameter in a course of irradiation, I_{pris} and I_{sat} are the parameter values for the pristine and strongly irradiated film (a leveling off behavior), respectively, Q is the cumulative charge delivered to the surface in coulombs, e is the electron charge, S_{irrad} is the area irradiated by the electron beam, and the cross-section σ (expressed here in cm^2) is a measure of a rate at which the saturation behavior is achieved. The expression (1) was used to fit both the decaying and increasing ($I_{pris} = 0$) parameters. The obtained values are compared with the previously found cross-sections for electron stimulated processes in AT SAMs.[18] We want to emphasize that the presented cross-sections only describe how fast the changes occur but not the extent of these changes. The latter parameters can be deduced from the presented experimental data.

5. Summary

The low energy (10 eV) electron induced damage in self-assembled monolayers formed from partially fluorinated alkanethiolates of F10H2SH, F10H11SH and F10H17SH on polycrystalline gold has been investigated *in-situ* by X-ray photoelectron spectroscopy and angle resolved near edge X-ray absorption fine structure spectroscopy. All investigated SFAT SAMs exhibit qualitatively similar behavior with respect to low energy electron irradiation. Both the fluorocarbon and hydrocarbon parts and the S/Au interface are affected simultaneously through the electron-induced dissociation of C–F, C–H, C–C, C–S and Au–thiolate bonds and the appearance of conformational and orientational defects. These processes result in progressive disordering of initially well-ordered, densely packed SAMs, desorption of film constituents, and chemical changes within the residual film. Whereas the film dehydrogenation could be followed only indirectly, the desorption of all other constituents could be quantitatively monitored. The noticeable desorption of sulfur-containing fragments, which probably include the complete SFAT chains, was only observed for F10H2S/Au. In general, however, desorbed carbon-containing fragments stem almost exclusively from the fluorocarbon part of the SFAT SAMs. The desorption of fluorine exceeds by $\approx 50\%$ carbon desorption, which implies that fluorine desorbs not only as a constituent of the carbon-containing fragments but through irradiation-induced scission of C–F bonds.

Chemical changes within the residual SFAT films include the complete disappearance of CF_3 moieties, partial transformation of CF_2 moieties into CF entities, complete loss of fluorine by some of the CF_2 groups, film dehydrogenation, appearance of C=C double bonds in both the fluorocarbon and hydrocarbon (predominately) parts, and transformation of the pristine thiolates into new irradiation-induced sulfur species assigned to disulfides and/or alkylsulfides.

Some general tendencies in the reaction of SAMs toward electron-irradiation can be deduced. First, whereas the entire SAM is damaged, the film/vacuum interface is predominately affected by irradiation-induced desorption processes. Second, the desorption of the complete molecules only occurs in short-chain films. Third, better ordered SAMs exhibit a higher stability toward electron irradiation.

Table 1 Cross-sections of the electron-irradiation induced processes in units of cm^2

	F10H2S/Au	F10H11S/Au	F10H17S/Au	ODT/Au
Cleavage of C–H bonds, conformational defects in the hydrocarbon chain		$(2.1 \pm 0.4) \times 10^{-16}$	$(2.2 \pm 0.4) \times 10^{-16}$	$(1.9 \pm 0.2) \times 10^{-16}$
Cleavage of C–F bonds, conformational defects in the fluorocarbon chain	$(1.7 \pm 0.3) \times 10^{-16}$	$(2.4 \pm 0.3) \times 10^{-16}$	$(2.4 \pm 0.3) \times 10^{-16}$	
Formation of C=C bonds	$(0.5 \pm 0.2) \times 10^{-16}$	$(1.2 \pm 0.2) \times 10^{-16}$	$(1.2 \pm 0.2) \times 10^{-16}$	$(0.85 \pm 0.1) \times 10^{-16}$
Desorption of fluorine	$(1.3 \pm 0.3) \times 10^{-16}$	$(1.7 \pm 0.3) \times 10^{-16}$	$(1.8 \pm 0.3) \times 10^{-16}$	
Reduction of CF_3 groups	$(3.0 \pm 0.3) \times 10^{-16}$	$(3.0 \pm 1.0) \times 10^{-16}$	$(3.0 \pm 1.0) \times 10^{-16}$	
Desorption of carbon containing fragments (thickness reduction)	$(1.8 \pm 0.3) \times 10^{-16}$	$(2.0 \pm 0.3) \times 10^{-16}$	$(1.8 \pm 0.3) \times 10^{-16}$	$(1.85 \pm 0.2) \times 10^{-16}$
Desorption of sulfur containing fragments	$(0.8 \pm 0.4) \times 10^{-16}$	$(0.3 \pm 0.2) \times 10^{-16}$	$(0.2 \pm 0.2) \times 10^{-16}$	$(0.27 \pm 0.04) \times 10^{-16}$ [$(0.8 \pm 0.1) \times 10^{-16}$]
Reduction of the thiolate species	$(2.0 \pm 0.6) \times 10^{-16}$	$(2.0 \pm 0.6) \times 10^{-16}$	$(2.0 \pm 0.6) \times 10^{-16}$	$(1.8 \pm 0.2) \times 10^{-16}$
Formation of irradiation-induced sulfur species	$(2.0 \pm 0.6) \times 10^{-16}$	$(1.8 \pm 0.6) \times 10^{-16}$	$(1.8 \pm 0.6) \times 10^{-16}$	$(1.7 \pm 0.2) \times 10^{-16}$

The presented values are a measure of a rate at which a saturation behavior is achieved. The first three lines are derived from the NEXAFS spectra and the residual cross-sections from the XPS data. The analogous cross-sections for SAMs formed from octadecanethiol (ODT) on Au are also presented for comparison.[18] In the case of sulfur containing fragments desorption the value for dodecanethiolate SAMs on gold is additionally shown in square brackets.[18]

References

1 B. Jäger, H. Schürmann, H. U. Müller, H.-J. Himmel, M. Neumann, M. Grunze and Ch. Wöll, *Z. Phys. Chem.*, 1997, **202**, 263.

2 M. Wirde, U. Gelius, T. Dunbar and D. L. Allara, *Nucl. Instrum. Methods Phys. Res., Sect. B*, 1997, **131**, 245.

3 M. Zharnikov, W. Geyer, A. Gölzhäuser, S. Frey and M. Grunze, *Phys. Chem. Chem. Phys.*, 1999, **1**, 3163.

4 R. C. Tiberio, H. G. Craighead, M. J. Lercel, T. Lau, C. W. Sheen and D. L. Allara, *Appl. Phys. Lett.*, 1993, **62**, 476.

5 M. J. Lercel, R. C. Tiberio, P. F. Chapman, H. G. Craighead, C. W. Sheen, A. N. Parikh and D. L. Allara, *J. Vac. Sci. Technol. B*, 1993, **11**, 2823.

6 M. J. Lercel, G. F. Redinbo, F. D. Pardo, M. Rooks, R. C. Tiberio, P. Simpson, H. G. Craighead, C. W. Sheen, A. N. Parikh and D. L. Allara, *J. Vac. Sci. Technol. B*, 1994, **12**, 3663.

7 M. J. Lercel, G. F. Redinbo, M. Rooks, R. C. Tiberio, H. G. Craighead, C. W. Sheen and D. L. Allara, *Microelectron. Eng.*, 1995, **27**, 43.

8 M. J. Lercel, M. Rooks, R. C. Tiberio, H. G. Craighead, C. W. Sheen, A. N. Parikh and D. L. Allara, *J. Vac. Sci. Technol. B*, 1995, **13**, 1139.

9 H. U. Müller, C. David, B. Völkel and M. Grunze, *J. Vac. Sci. Technol. B*, 1995, **13**, 2846.

10 C. David, H. U. Müller, B. Völkel and M. Grunze, *Microelectron. Eng.*, 1996, **30**, 57.

11 M. J. Lercel, H. G. Craighead, A. N. Parikh, K. Seshadri and D. L. Allara, *Appl. Phys. Lett.*, 1996, **68**, 1504.

12 R. Hild, C. David, H. U. Müller, B. Völkel, D. R. Kayser and M. Grunze, *Langmuir*, 1998, **14**, 342.

13 W. Geyer, V. Stadler, W. Eck, M. Zharnikov, A. Gölzhäuser and M. Grunze, *Appl. Phys. Lett.*, 1999, **75**, 2401.

14 P. E. Laibinis, R. L. Graham, H. A. Biebuyck and G. M. Whitesides, *Science*, 1991, **254**, 981.

15 P. Rowntree, P.-C. Dugal, D. Hunting and L. Sanche, *J. Phys. Chem.*, 1996, **100**, 4546.

16 C. Olsen and P. A. Rowntree, *J. Chem. Phys.*, 1998, **108**, 3750.

17 H. U. Müller, M. Zharnikov, B. Volkel, A. Schertel, P. Harder and M. Grunze, *J. Phys. Chem. B*, 1998, **102**, 7949.

18 M. Zharnikov, S. Frey, K. Heister and M. Grunze, *Langmuir*, 2000, **16**, 2697.

19 K. Heister, S. Frey, A. Gölzhäuser, A. Ulman and M. Zharnikov, *J. Phys. Chem. B*, 1999, **103**, 11098.

20 A. Ulman, *An Introduction to Ultra-thin Organic Films: Langmuir-Blodgett to Self-Assembly*, Academic Press, New York, 1991; A. Ulman, *Chem. Rev.*, 1996, **96**, 1533.

21 H. Sellers, A. Ulman, Y. Scnidman and J. E. Eilers, *J. Am. Chem. Soc.*, 1993, **115**, 9389.

22 *Thin films: self-assembled monolayers of thiols*, ed. A. Ulman, Academic Press, San Diego, 1998.

23 P. Fenter, P. Eisenberger and K. S. Liang, *Phys. Rev. Lett.*, 1993, **70**, 2447.

24 P. Fenter, A. Eberhardt and P. Eisenberger, *Science*, 1994, **266**, 1216.

25 (*a*) N. Camillone, C.E.D. Chidsey, G. Liu and G. Scoles, *J. Chem. Phys.*, 1993, **98**, 3503; (*b*) N. Camillone, C. E. D. Chidsey, G. Liu and G. Scoles, *J. Chem. Phys.*, 1993, **98**, 4234.

26 G. E. Poirier and M. J. Tarlov, *Langmuir*, 1994, **10**, 2853.

27 E. Delmarche, B. Michel, H. A. Biebuyck and G. Gerber, *Adv. Mater.*, 1996, **8**, 719.

28 C. A. Alves and M. D. Porter, *Langmuir*, 1993, **9**, 3507.

29 D. G. Castner, K. B. Lewis, D. A. Fischer, B. D. Ratner and J. L. Gland, *Langmuir*, 1993, **9**, 537.

30 T. J. Lenk, V. M. Hallmark, C. L. Hoffmann, J. F. Rabolt, D. G. Castner, C. Erdelen and H. Ringsdorf, *Langmuir*, 1994, **10**, 4610.

31 G.-Y. Liu, P. Fenter, C. E. D. Chidsey, D. F. Ogletree, P. Eisenberger and M. Salmeron, *J. Chem. Phys.*, 1994, **101**, 4301.

32 M.-W. Tsao, C. L. Hoffmann and J. F. Rabolt, *Langmuir*, 1997, **13**, 4317.

33 M. Monduzzi, *Curr. Opin. Colloid Interface Sci.*, 1998, **3**, 467.

34 K. Tamada, J. Nagasawa, F. Nakanishi, K. Abe, M. Hara, W. Knoll, T. Ishida, H. Fukushima, S. Miyashita, T. Usui, T. Koini and T. R. Lee, *Thin solid films*, 1998, **327–329**, 150.

35 K. Tamada, T. Ishida, W. Knoll, H. Fukushima, T. Koini and T. R. Lee, in preparation.

36 S. Frey, K. Heister, M. Zharnikov and M. Grunze, *Israel J. Chem.* (special issue), in the press.

37 M. Graupe, T. Koini, V. Wang, G. M. Nassif, R. Colorado, Jr., R. J. Villazana, H. Dong, Y. F. Miura, O. E. Shmakova and T. R. Lee, *J. Fluorine Chem.*, 1998, **93**, 107.

38 L. Strong and G. M. Whitesides, *Langmuir*, 1988, **4**, 546.

39 S. Bernstorff, W. Braun, M. Mast, W. Peatman and T. Schröder, *Rev. Sci. Instrum.*, 1989, **60**, 2097.

40 J. Stöhr, *NEXAFS Spectroscopy*, Springer Series in Surface Science 25, Springer-Verlag, Berlin–Heidelberg, 1992.

41 P. E. Batson, *Phys. Rev. B*, 1993, **48**, 2608.

42 J. F. Moulder, W. E. Stickle, P. E. Sobol and K. D. Bomben, *Handbook of X-ray Photoelectron Spectroscopy*, ed. J. Chastian, Perkin-Elmer Corporation, Eden Prairie, MN, 1992.

43 D. A. Shirley, *Phys. Rev. B*, 1972, **5**, 4709.

44 G. K. Wertheim, M. A. Butler, K. W. West and D. N. E. Buchanan, *Rev. Sci. Instrum.*, 1974, **45**, 1369.

45 C. D. Bain and G. M. Whitesides, *J. Phys. Chem.*, 1989, **93**, 1671.

46 P. Harder, M. Grunze, R. Dahint, G. M. Whitesides and P. E. Laibinis, *J. Phys. Chem.*, 1998, **102**, 426.

47 J. Thome, M. Himmelhaus, M. Zharnikov and M. Grunze, *Langmuir*, 1998, **14**, 7435.

48 T. Ohta, K. Seki, T. Yokoyama, I. Morisada and K. Edamatsu, *Phys. Scr.*, 1990, **41**, 150.

49 G. Hähner, M. Kinzler, Ch. Wöll, M. Grunze, M. Scheller, L. S. Cederbaum, *Phys. Rev. Lett.*, 1991, **67**, 851; erratum, *Phys. Rev. Lett.*, 1992, **69**, 694.

50 P. S. Bagus, K. Weiss, A. Schertel, Ch. Wöll, W. Braun, H. Hellwig and C. Jung, *Chem. Phys. Lett.*, 1996, **248**, 129.

51 P. Väterlein, R. Fink, E. Umbach and W. Wurth, *J. Phys. Chem.*, 1998, **108**, 3313.

52 D. A. Outka, J. Stöhr, J. P. Rabe and J. D. Swalen, *J. Chem. Phys.*, 1988, **88**, 4076.

53 G. Hähner, M. Kinzler, C. Thümmler, Ch. Wöll and M. Grunze, *J. Vac. Sci. Technol.*, 1992, **10**, 2758.

54 G. Beamson and D. Briggs, *High Resolution XPS of Organic Polymers*, John Wiley & Sons, Chichester, 1995.

55 H. Rieley, G. K. Kendall, F. W. Zemicael, T. L. Smith and S. Yang, *Langmuir*, 1998, **14**, 5147.